Oxidation of pyridine nucleotides during Fas- and ceramide-induced apoptosis in Jurkat cells: correlation with changes in mitochondria, glutathione depletion, intracellular acidification and caspase 3 activation

Patrice Xavier PETIT*[1], Marie-Claude GENDRON†, Nicolas SCHRANTZ‡, Didier MÉTIVIER§, Guido KROEMER§, Zofia MACIOROWSKA‖, Franck SUREAU* and Steven KOESTER¶

*Institut Cochin de Génétique Moléculaire, INSERM U129, CHU Cochin Port-Royal, 24 rue du Faubourg Saint-Jacques, F-75014 Paris, France, †Service de Cytométrie en Flux, Institut Jacques Monod, Université Denis Diderot, 4 place Jussieu, F-75005 Paris, France, ‡INSERM U131, IPSC, 32 rue des Carnets, 92140 Clamart, France, §Centre National de la Recherche Scientifique, UPR 420, 19 rue Guy Môquet, F-94801 Villejuif, France, ‖Institut Curie, Département de Pathologie, 26 rue d'Ulm, 75248 Paris Cedex 05, France, and ¶Beckman Coulter, Inc., Advanced Technology, 11800 S.W. 147th Avenue, Miami, FL 33196-2500, U.S.A.

Jurkat T cells showed a major, early decrease in blue autofluorescence in response to Fas/Apo-1/CD95 cross-linking or stimulation with cell-permeant ceramide. This indicates the oxidation/depletion of NADH or NADPH before the onset of apoptosis. Kinetic studies, cytofluorimetric multiparameter analyses and cell sorting experiments indicated a close temporal relationship between NAD(P)H oxidation/depletion and the dissipation of the mitochondrial transmembrane potential ($\Delta\Psi_m$). In contrast, NAD(P)H depletion was detected well before several other changes associated with late apoptosis, including enhanced superoxide generation, phosphatidylserine exposure on the cell surface, loss of cytosolic K^+, decreased cytoplasmic pH, nuclear DNA fragmentation, cell shrinkage, loss of viability and the appearance of the mitochondrial antigen APO2.7. Full activation of caspase 9 and caspase 3 appeared to be correlated with the appearance of superoxide anions in the mitochondria, and followed the drop in NADPH. Overexpression of the apoptosis-inhibitory proto-oncogene Bcl-2, which encodes an inhibitor of the mitochondrial permeability transition (PT) pore, delayed both the $\Delta\Psi_m$ disruption and the depletion of NAD(P)H. Similar effects were observed with the pharmacological PT pore inhibitors, bongkrekic acid and cyclosporin A. Thus there appears to be a close functional relationship between mitochondrial and cellular redox changes during early apoptosis; events that are inhibited by Bcl-2.

Key words: Bcl-2, cell death, mitochondrial transmembrane potential, permeability transition, redox status.

INTRODUCTION

While the division of apoptosis into three functionally distinct phases [1–5] is artificial, it provides an attractive theoretical framework for studies on apoptotic pathways. The pre-mitochondrial initiation phase is extremely heterogeneous and includes the transduction of several signal and damage pathways that are 'specific' in the sense that they are not universally activated, but depend on the death-inducing primary stimulus and/or cell type. These pathways converge on the mitochondrion, which integrates them into a common pathway. The common mitochondrial phase marks the 'decision to die', which involves the irreversible loss of mitochondrial-membrane barrier function [1–5]. Thus the inner mitochondrial transmembrane potential ($\Delta\Psi_m$) is frequently lost during the early phase of apoptosis [6–9], and the outer mitochondrial membrane becomes permeable, leading to the release of soluble intermembrane proteins into the cytosol [10–14].

It is only after this process, beyond the point-of-no-return, that downstream caspases, such as caspases 9 and 3, are activated and endonucleases subsequently come into action, leading to the acquisition of the biochemical and morphological hallmarks of apoptosis [15,16]. The decisive step in apoptosis is thus mitochondrial-membrane permeabilization, which is mediated by the permeability transition (PT) pore complex (PTPC), at least in certain cases [17]. The PTPC is a multiprotein complex at the contact site between the inner and the outer mitochondrial membranes; it may control the permeability of the inner and/or outer mitochondrial membranes [18–20]. The importance of the PTPC in the regulation of apoptosis was underscored recently by the discovery that it is directly controlled by both the pro- and the anti-apoptotic members of the Bax/Bcl-2 family [20–22]. The function of the PT pore has been extensively analysed, and it is now clear that intramitochondrial anti-oxidants, such as GSH, NADH, NADPH and manganese-dependent superoxide dismutase, are endogenous inhibitors of PT pore opening [23–26]. The NAD(P)H concentrations also appear to be reduced in several models of cell death [27,28]. Conditions in which the NADH concentration is elevated have been reported to prevent PT pore opening [29], and in some instances [30,31] may also prevent apoptosis. Conversely, the opening of the PT pore results in uncoupling of the respiratory chain, and interruption of electron transfer due to the release of cytochrome *c* with overproduction of superoxide anions [32]. The opening of the PT

Abbreviations used: Ac-DEVD-CHO, acetyl-Asp-Glu-Val-Asp-aldehyde; BA, bongkrekic acid; αCD95, CD95-specific IgM antibody; CsA, cyclosporin A; $\Delta\Psi_m$, mitochondrial transmembrane potential; DAPI, 4′,6-diamidino-2-phenylindole; $DiOC_6(3)$, 3,3′-dihexyloxacarbocyanine iodide; Eth, ethidium; FCS, fetal calf serum; HE, hydroethidine; JC-1, 5,5′,6,6′-tetrachloro-1,1′,3,3′-tetraethylbenzimidazol carbocyanine iodide; MCB, monochlorobimane; PARP, poly(ADP-ribose) polymerase; PBFI/AM, benzofuran isophthalate-acetoxymethyl ester; PT, permeability transition; PTPC, PT pore complex; ROS, reactive oxygen species; SNARF-1/AM, 5-(and-6-)-carboxy-seminaphthorhodafluor-1 acetoxymethyl ester acetate; Z-VAD-FMK, benzyloxycarbonyl-Val-Ala-DL-Asp-fluoromethylketone.

[1] To whom correspondence should be addressed (e-mail pxpetit@icgm.cochin.inserm.fr).

pore also causes rapid oxidation/depletion of GSH [33], which is in redox equilibrium with NAD(P)H [34].

While oxidative processes can stimulate PT pore opening, PT pore opening results in the loss of redox detoxifying reactions and the overproduction of reactive oxygen species (ROS). We have therefore measured the intracellular NAD(P)H concentration during apoptosis. We have also collected information on the relationship between the apoptotic depletion of NAD(P)H and a number of mitochondrial and extra-mitochondrial parameters said to be altered during apoptosis, with particular emphasis on redox processes. Our findings point to a close temporal and functional relationship between NAD(P)H depletion, loss of the $\Delta\Psi_m$ that preceded caspase 3 activation (and intracellular acidification, which clearly takes part in the enhancement of caspase 9 and caspase 3 activation) and related changes in cellular redox processes (with GSH depletion).

EXPERIMENTAL

Cell lines and culture conditions

Wild-type Jurkat cells ($2–5 \times 10^5$/ml) were obtained from the A.T.C.C., and were cultured in complete medium [RPMI 1640 medium supplemented with 10 % (v/v) fetal calf serum (FCS), L-glutamine and antibiotics] with or without 1 μg/ml CD95-specific IgM antibody (αCD95; CH-11; Immunotech, Marseille, France) or 50 μM C2-ceramide (Sigma) for periods of 3–24 h. The ligand of the adenine nucleotide translocator, bongkrekic acid (BA; 50 μM final concentration; provided by Dr J. A. Duine, Delft University, Delft, The Netherlands), or cyclosporin A (CsA; 1 μM final concentration; Novartis, Basel, Switzerland) were added to the cultures 15 min before αCD95. Jurkat cells transfected with the human Bcl-2 gene or a control vector containing only the neomycin resistance gene were used in some experiments.

Determination of NAD(P)H autofluorescence

Fluoresence was elicited with an argon laser (488 nm at 100 mW) and multiline ultraviolet light at 400 mW. Changes in the autofluorescence of normal and apoptotic cells were recorded. The light emitted was collected with a 424 ± 40 nm bandpass for the NAD(P)H fluorescence [35,36]. Data were analysed in triplicate and results for 10000 cells were acquired with gating on cells exhibiting normal forward-scatter and side-scatter characteristics, or on the whole cell population (normal and shrunken cells), as indicated. In one experiment, cells were sorted using a FACS Vantage cytofluorimeter (Becton–Dickinson, San Jose, CA, U.S.A.), based on NAD(P)H autofluorescence. Cells were sorted into complete medium enriched with 20 % (v/v) FCS, kept on ice and re-analysed within 30 min.

HPLC determination of the oxidized and reduced pyridine (nicotinamide) nucleotides and adenylates in extracts of normal and apoptotic cells

Reverse-phase chromatography was performed [37] to evaluate the oxidized and reduced pyridine nucleotides and the adenylates in extracts of control cells and of cells incubated for 8 h with 1 μg/ml αCD95. The phenol/chloroform/isoamyl alcohol method [38] was modified [37] to include a second diethyl ether extraction step. Aliquots (1 ml) of cell suspensions (5 mg of protein/ml) were quickly added to ice-cold phenol/chloroform/isoamyl alcohol (34:24:1, by vol.) containing 0.6 ml of aqueous 66 mM EDTA (pH 7.4), and the mixture was shaken vigorously for 90 s. It was then centrifuged for 10 min at 900 ***g*** to separate the phases. The upper phase (1.1 ml) was withdrawn and extracted twice with 1 ml of water-saturated diethyl ether by shaking for 30 s and removing the lower aqueous phase with a Pasteur pipette. The aqueous phase was frozen in liquid nitrogen and stored until HPLC analysis. The identity of the peaks was checked by co-elution with authentic standards (Sigma).

Determination of changes in mitochondria and mitochondrial superoxide anion generation

$\Delta\Psi_m$ and superoxide anion generation were evaluated by incubating cells (5×10^5/ml) with 2.5 nM 3,3′-dihexyloxacarbocyanine iodide [$DiOC_6(3)$; Molecular Probes, Eugene, OR, U.S.A.; 1 μM stock solution dissolved in ethanol] [7,39] and 1 μM hydroethidine (HE; Molecular Probes; 500 μM stock solution) for 15 min at 37 °C. Cells were analysed using a FACS Vantage cytofluorometer (Becton–Dickinson), gating the forward- and side-scatter to exclude debris. The fluorescence was excited with an argon laser (excitation wavelength 488 nm) and collected using a bandpass of 530 ± 30 nm for $DiOC_6(3)$, or a bandpass of 585 ± 20 nm for HE, after suitable compensation. A minimum of 5×10^3 events were acquired in list mode and were analysed with Cellquest™ software (Becton–Dickinson). Cells were stained with 5,5′,6,6′-tetrachloro-1,1′,3,3′-tetraethylbenzimidazol carbocyanine iodide (JC-1) as described by Kühnel et al. [40]. Cells to be stained with the FITC–APO2.7 conjugate (Immunotech) were permeabilized with 100 μg/ml digitonin (Sigma) and were washed two times with PBS (pH 7.2) containing 20 mg/ml BSA following the manufacturer's protocol (Immunotech) and Koester et al. [41].

Cytofluorimetric determination of other apoptosis-associated alterations

The cell content of GSH was determined using 50 μM monochlorobimane (MCB; 100 mM stock solution dissolved in ethanol). Intracellular K^+ was measured by loading cells for 15–30 min with 2.5 μM cell-permeant benzofuran isophthalate-acetoxymethyl ester (PBFI/AM; 500 μM stock solution dissolved in dimethylformamide) [42,43]. PBFI fluorescence was excited at 360 nm and collected at 485 ± 20 nm. Exposed phosphatidylserine on the outer plasma membrane was measured by staining cells with 1 μg/ml annexin V-FITC for 10 min at 4 °C (Immunotech). The pH within single cells was monitored with the fluorescent pH indicator 5-(and-6-)-carboxy-seminaphthorhodafluor-1 acetoxymethyl ester acetate (SNARF-1/AM) [44], whose emission spectrum has two pH-sensitive bands: the band corresponding to the protonated form (590 nm) and the band corresponding to the unprotonated forms (635 nm). Its pK is approx. 7.4, so that pH changes in the 6.3–8.6 range can be determined by measuring the ratio of the fluorescence at 635 nm over the fluorescence at 590 nm. Cells to be loaded with the fluorescent probes were incubated in culture medium for 20 min at 37 °C, 5 % CO_2, with 10 μM SNARF-1/AM (1 mM stock solution dissolved in DMSO), loaded with probe, washed and suspended in culture medium containing 25 mM Hepes (pH 7.4) before flow cytometric measurements. An *in vivo* calibration curve of *R* versus intracellular pH was prepared [45]. Briefly, cells incubated with SNARF-1/AM were washed and suspended in buffer (10 mM Hepes, 130 mM KCl, 20 mM NaCl, 5 mM dextrose, 1 mM $CaCl_2$, 1 mM KH_2PO_4 and 0.5 mM $MgSO_4$) at various pH values, obtained by adding small amounts of 0.1 M KOH or HCl. The pH changes outside the cell were monitored with a Tacussel pH meter. Nigericin (1 μg/ml) and valinomycin (5 μM) were added to exchange K^+ for H^+, which resulted in the rapid equilibration of external and internal pHs, over the pH

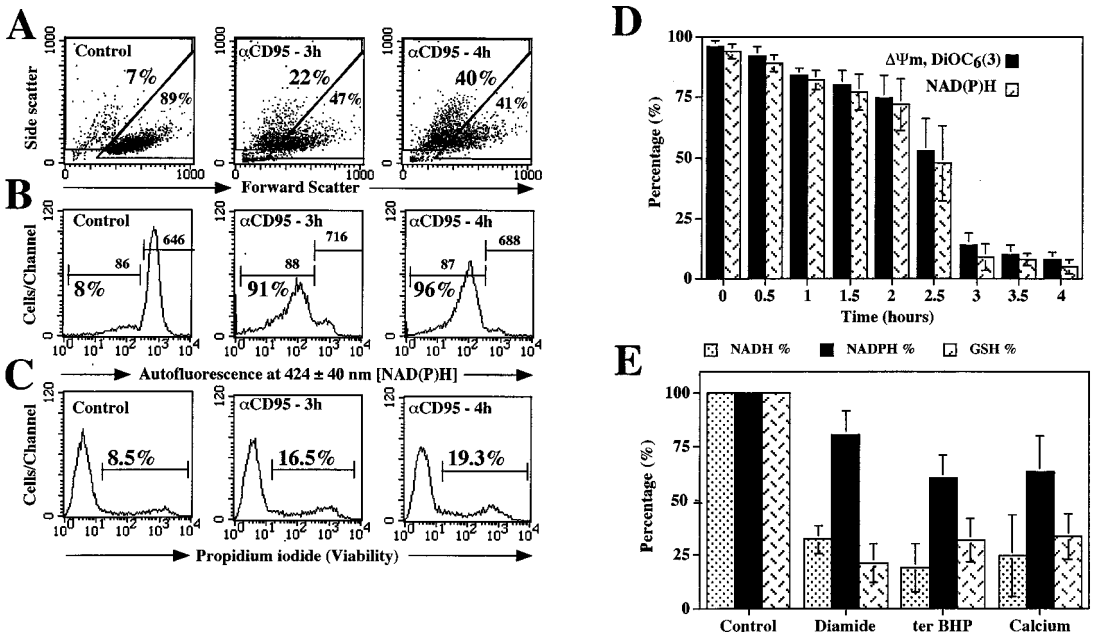

Figure 1 Early NAD(P)H depletion during apoptosis

Jurkat cells were cultured for 3–4 h with or without 0.1 μg/ml αCD95, and the following parameters were assessed: forward-scatter compared with side-scatter (**A**); autofluorescence at 424 $\pm$ 40 nm (**B**); and uptake of the vital dye propidium iodine (**C**). Similar results were obtained in three independent experiments. (**D**) Time course of decreases in $DiOC_6(3)$ and NAD(P)H fluorescence during CD95-induced apoptosis. (**E**) The mitochondrial NAD(P)H content was measured in isolated mouse-liver mitochondria treated with 50 μM diamide, 300 μM calcium or 10 μM *t*-butylhydroperoxide (ter BHP) in order to open the PT pore [26]. Under these conditions, *t*-butylhydroperoxide did not permeabilize the mitochondrial outer membrane by oxidizing lipids, but specifically affected PT pore opening [13]. In isolated mouse-liver mitochondria the values of NADH, NADPH and GSH were 1.6 $\pm$ 0.3, 2.7 $\pm$ 0.4 and 4.0 $\pm$ 0.5 nmol/mg of protein respectively (means $\pm$ S.D. for 10 independent measurements). The reaction was started by adding mitochondria to 0.5 μM CsA to avoid non-specific opening of the PT pore [26].

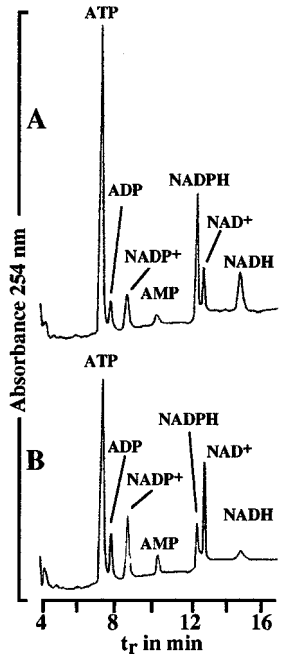

Figure 2 HPLC determination of the NAD(P)H and ATP/ADP ratio of apoptotic cells

Chromatographs of phenol extracts [38] of untreated Jurkat cells (**A**) or Jurkat cells incubated for 4 h with 1 μg/ml αCD95. Of the treated cells 92% had a low $\Delta\Psi_m$ (see Figure 5) and a reduced NAD(P)H fluorescence by flow cytometry. Cell extracts (5 mg/ml) were extracted and separated by reverse-phase chromatography. t_r, HPLC running time.

range studied (6.0–8.0). Cell viability was not significantly affected by adding nigericin or valinomycin, or by loading with SNARF-1/AM. The cell-permeable fluorogenic substrate Phiphilux G1D2 (OncoImmunin, Inc., Kensington, MD, U.S.A.) containing the sequence GDEVDG (single-letter amino acid notation) was used to detect caspase-3-like activity in intact cells by flow cytometry. Cells were cultured with or without 1 μg/ml αCD95. They were subsequently harvested and were washed twice in PBS. Cells (1×10^6) were resuspended in 50 μl of substrate solution and were incubated for 1 h at 37 °C in the dark. They were then washed and suspended in PBS; the fluorescence emission at 530 $\pm$ 30 nm was measured using a FACS Vantage cytofluorimeter (Becton–Dickinson). When 50 μM benzyloxycarbonyl-Val-Ala-DL-Asp-fluoromethylketone (Z-VAD-FMK) and 100 μM acetyl-Asp-Glu-Val-Asp-aldehyde (Ac-DEVD-CHO) were used (Alexis Biochemicals), cells were incubated before inducing apoptosis. The frequency of hypoploid cells was determined by fixing cells with ethanol and staining them with propidium iodide [46], using an EPICS Profile II Analyzer (Coulter, Miami, FL, U.S.A.). All other stainings were analysed using a FACS Vantage cytofluorimeter (Becton–Dickinson).

Western-blot analysis

Cells were lysed by incubation with modified Laemmli's buffer [60 mM Tris (pH 6.8), 10% (v/v) glycerol and 2% (w/v) SDS, without 2-mercaptoethanol and Bromophenol Blue], were disrupted by sonication for 30 s on ice and were then centrifuged at 3000 ***g*** for 5 min. The supernatants were boiled for 5 min at

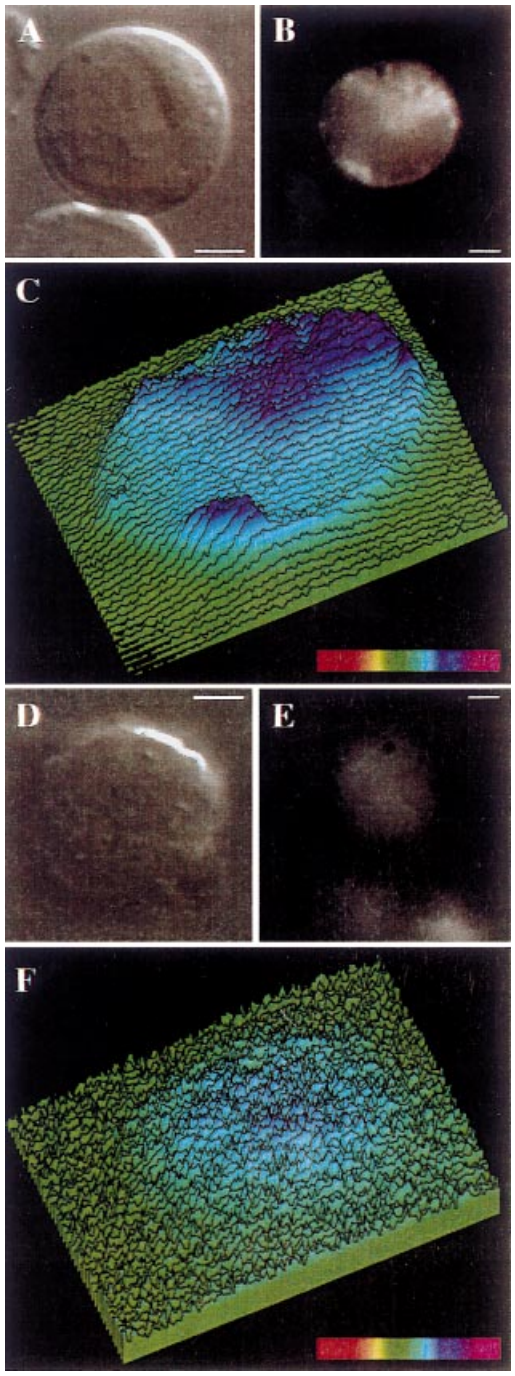

Figure 3 Videomicroscopy of NADPH

Control cells (**A**, **B** and **C**) and αCD95-treated cells (0.1 μg/ml for 3 h) (**D**, **E** and **F**) were analysed for transmitted light (**A** and **D**), and fluorescence of NAD(P)H with a DAPI filter set (**B** and **E**). The area plots for (**B** and **E**) are shown in (**C** and **F**). Bars represent 5 μm. The coloured bars in (**C** and **F**) show the NADPH fluorescence, from high fluorescence (violet) to low fluorescence (green).

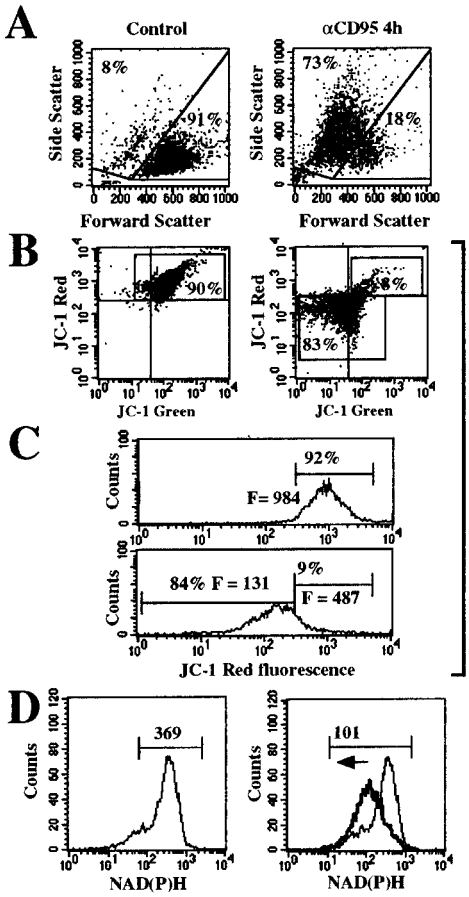

Figure 4 Relationship between cell shrinkage, NAD(P)H depletion and $\Delta\psi_m$ dissipation determined by JC-1 staining

Untreated cells (left-hand panels) or cells treated with 1 μg/ml αCD95 for 4 h (right-hand panels) were stained with JC-1 and analysed for forward-scatter and side-scatter chacteristics (**A**), green compared with red JC-1 fluorescence (**B**), monoparametric analysis of the red fluorescence (**C**) and NAD(P)H autofluoresence (**D**). Numbers refer to the percentages of cells in a given window, or to the mean fluorescence channel (F = log scale). The values in (**C**) are extracted from (**B**), and both representations are linked by a line on the right-hand side of the Figure.

100 °C and frozen at −80 °C or used immediately. Aliquots of the supernatant were assayed for protein concentration (micro-BCA protein assay; Pierce, Rockford, IL, U.S.A.). Cell lysate proteins (20 μg/lane) were resolved by SDS/PAGE [7.5% or 15% (w/v) polyacrylamide]. Proteins were then electroblotted on to 0.45 μm pore-size nitrocellulose filters, and the filters were blocked by incubation with 5% (w/v) non-fat milk in PBS containing 0.1% Tween-20 for 1 h. The filters were then incubated for 1 h at room temperature with 1 μg/ml anti-(caspase 3) (polyclonal rabbit anti-(caspase 3) serum; Pharmingen, San Diego, CA, U.S.A.), anti-(caspase 9) rabbit serum (provided by Dr X. Wang), or poly(ADP-ribose) polymerase (PARP) monoclonal antibody C2.10 (1 μg/ml) (purchased from Dr G. G. Poirier, Wellcome/CRC Institute of Cancer and Developmental Biology, Cambridge, U.K.). Blots were washed three times for 10 min with 0.2% Tween 20 in PBS, and were subsequently incubated for 1 h with peroxidase-labelled anti-mouse or anti-rabbit immunoglobulins (at 1:5000 dilution). Blots were developed using an enhanced chemiluminescence detection system (ECL®; Amersham).

Videomicroscopy of NAD(P)H fluorescence

This study was performed with a computer-assisted image analysis system (Quantum, Appligene, Illkirch, France), coupled to a black and white CCD camera (where CCD stands for cooled camera device; C2400; Hamamatsu, Bridgewater, NJ, U.S.A.), a

cooled low-level CCD camera (CH250; Photometrics, Waterloo, Canada) and an inverted microscope (Axiovert 135; Zeiss, Oberkochen, Germany). Images were acquired with a 100:1.3 oil immersion objective (Plan-NEOFLUAR; Zeiss) with a 1.6 zoom factor (Optovar 2). Transmitted light images were acquired with the C2400 camera in Differential Interference Contrast ('DIC') mode. Fluorescence images were digitized with the CH250 camera using the 4′,6-diamidino-2-phenylindole (DAPI) filter set (i.e. a 365 ± 12 nm bandpass excitation filter, a 395 nm beam splitter and a 397 nm long pass emission filter). Transmitted images were digitized in a 512×474 array on 8 bits, and fluorescent images were digitized in a 512×512 array on 12 bits. The images were exported in 8-bit TIFF format. Scion Image software (Scion Corporation, Frederick, MD, U.S.A.) was used to make the area plots, and Photoshop 5.0 software (Adobe Systems Incorporated) was used to generate prints on a sublimation printer (ColorEase PS printer, Kodak).

RESULTS AND DISCUSSION

Oxidation of mitochondrial pyridine nucleotides during early apoptosis

The fluorescence of reduced pyridine nucleotides (NADH and NADPH) accounts for most of the cell autofluorescence excited by near UV light, and it comes almost exclusively from mitochondria [27]. Oxidized pyridine nucleotides (NAD^+ and $NADP^+$) do not fluoresce. Accordingly, changes in autofluorescence reflect changes in the redox state of pyridine nucleotides. We monitored the oxidation of pyridine nucleotides during early apoptosis by analysing UV-excited Jurkat T cells that had been incubated with αCD95 for 3–4 h. This incubation perturbs mitochondrial function but does not result in advanced apoptosis (i.e. nuclear condensation, DNA fragmentation or perturbations of phosphatidylserine at the plasma membrane) [47–49]. A portion of the cells acquired 'apoptotic' light-scattering characteristics, indicating shrinkage (Figure 1A). Most cells, however, showed a major decrease in autofluorescence at 424 nm, indicating the oxidation/depletion of NAD(P)H. Thus a major change in cellular redox potentials occurs early in apoptosis (Figure 1B), before cells shrink (Figure 1A) and lose their capacity to exclude the vital stain propidium iodide (Figure 1C). Only 22% of the cells had shrunk at 3 h (16.5% had lost viability), whereas 91% exhibited a low NAD(P)H fluorescence (Figure 1A). Monitoring the changes in $\Delta\Psi_m$ and NAD(P)H oxidation revealed slight decreases in both, at 1 h, with a clear drop at 2 h; the lowest value was obtained at 3 h (Figure 1D).

This change also appears to be similar to the loss of NADPH fluorescence by isolated mitochondria incubated with calcium, diamide or *t*-butylhydroperoxide (Figure 1E) in order to change the permeability. Determination of NADH and NAD(P)H, in cellular extracts from normal and apoptotic cells, using HPLC provided supporting information. Figure 2 shows typical chromatograms of normal and apoptotic Jurkat cells (8 h after induction with 1 μg/ml αCD95). The chromatography conditions separated the three adenylates and the four species of pyridine nucleotides. The difference in the NADPH and NADH contents of normal and apoptotic cells can be seen. It is clear that NADH and NADPH are oxidized during apoptosis. These changes were also associated with a marked decrease in the ATP/ADP ratio, from 10 in normal cells to 4 in apoptotic cells.

Control Jurkat cells had high NAD(P)H fluorescence and appeared to be normal (Figures 3A, 3B and 3C). Jurkat cells incubated with αCD95 for 3 h had very low NAD(P)H fluorescence (Figures 3E and 3F) and a condensed morphology

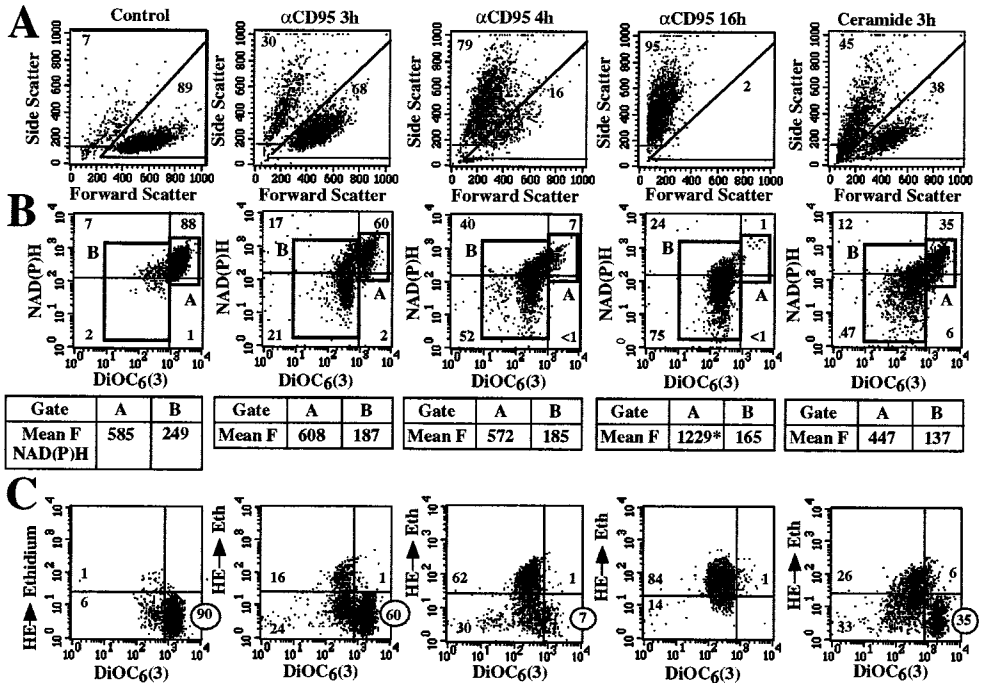

Figure 5 Relationship between NAD(P)H depletion, $\Delta\Psi_m$ dissipation and overproduction of superoxide anions

Jurkat cells were cultured for the indicated periods with 0.5 μg/ml αCD95, and then stained with $DiOC_6(3)$ and HE. The parameters measured are: forward-scatter and side-scatter characteristics (**A**); NAD(P)H autofluorescence versus $DiOC_6(3)$ staining (**B**); and HE versus $DiOC_6(3)$ staining (**C**). *Indicates the few cells escaping to death, which are of high NAD(P)H fluorescence (they represent < 1% of the cells).

typical of the early morphological changes associated with apoptosis (Figure 3D). The changes were not pronounced, because these events take place at an early stage when the permeability of the plasma membrane to propidium iodide is not affected and when no aberrant exposure of phosphatidylserine residues on the outer leaflet of the membrane can be seen.

Relationship between $\Delta\Psi_m$ dissipation and NAD(P)H oxidation

Since the collapse of $\Delta\Psi_m$ is one of the first alterations that accompanies early apoptosis [6,7], we determined the temporal relationship between the loss of $\Delta\Psi_m$ and NAD(P)H oxidation. Jurkat cells were stained with JC-1 to obtain information on the mitochondrial 'mass' (green fluorescence) and on $\Delta\Psi_m$ (red fluorescence) (Figures 4A and 4C). Treating cells with αCD95 for 4 h decreased $\Delta\Psi_m$ in a significant portion of cells (Figure 4B) without affecting the mitochondrial 'mass', provided that the plasma membrane was not affected (results not shown). The dissipation of $\Delta\Psi_m$ also affected cells with normal light-scatter characteristics (see the difference between the 73% of cells with low-forward-light scatter and the 83% of cells with low $\Delta\Psi_m$), indicating that it occurs before shrinkage [7]. Similarly, the NAD(P)H-dependent autofluoresence was reduced in the majority of cells treated for 4 h with αCD95 (Figure 4D).

Cells were stimulated with αCD95, or the pro-apoptotic second messenger ceramide, and then stained with the $\Delta\Psi_m$-sensitive dye $DiOC_6(3)$ and HE to further clarify the relationship between $\Delta\Psi_m$ dissipation and NAD(P)H oxidation, (Figure 5). HE is cell permeant and can be oxidized by superoxide anions to ethidium (Eth), a fluorescent dye that is retained by the cells. Therefore the conversion of HE into Eth provides an estimate of superoxide anion generation in the cell [50]. $DiOC_6(3)$/HE double-staining [8] identifies cells with normal characteristics [$DiOC_6(3)^{high}$(HE $\rightarrow$ Eth)^{low} cells, stage I], cells in early apoptosis [$DiOC_6(3)^{low}$ (HE $\rightarrow$ Eth)^{low} cells, stage II] and cells in a more advanced stage [$DiOC_6(3)^{low}$(HE $\rightarrow$ Eth)^{high} cells, stage III] (Figure 5C). The NAD(P)H-dependent autofluorescence of each of these subpopulations indicated that all $DiOC_6(3)^{low}$ cells had a low NAD(P)H content, irrespective of their HE $\rightarrow$ Eth status (Figures 5B and 5C). This suggests a correlation between the dissipation of $\Delta\Psi_m$ and NAD(P)H oxidation.

We performed a control experiment in which cells stimulated for 3 h with αCD95 were, without any prior staining, separated based on their NAD(P)H autofluorescence into NAD(P)H^{high} and NAD(P)H^{low} cells (Figures 6A and 6B). These fractions were stained with $DiOC_6(3)$. Almost all of the NAD(P)H^{high} cells were $DiOC_6(3)^{high}$, whereas almost all of the NAD(P)H^{low} cells were $DiOC_6(3)^{low}$ (Figure 6C). Hence, the two parameters, NAD(P)H and $\Delta\Psi_m$, are perturbed simultaneously, during early apoptosis.

Relationship between NAD(P)H oxidation, GSH status, intracellular pH, ROS overgeneration, loss of plasma membrane asymmetry and K^+ efflux

The multiparameter analyses shown in Figure 6 demonstrate that cells were depleted of NAD(P)H well before any enhanced generation of superoxide anions was detectable by the HE $\rightarrow$ Eth oxidation method. Similarly, cells incubated with αCD95 and purified on NAD(P)H^{low} were mostly (HE $\rightarrow$ Eth)^{low} (Figure 6C). This means that the proportion of cells with low NAD(P)H fluorescence corresponded strictly to the cells with low $\Delta\Psi_m$, as only 17% of them produced superoxide anions. In contrast, the intracellular concentration of GSH, measured by the GSH-sensitive dye MCB, declined with the loss of NAD(P)H (Figure 6D). This was also true for changes in the intracellular pH

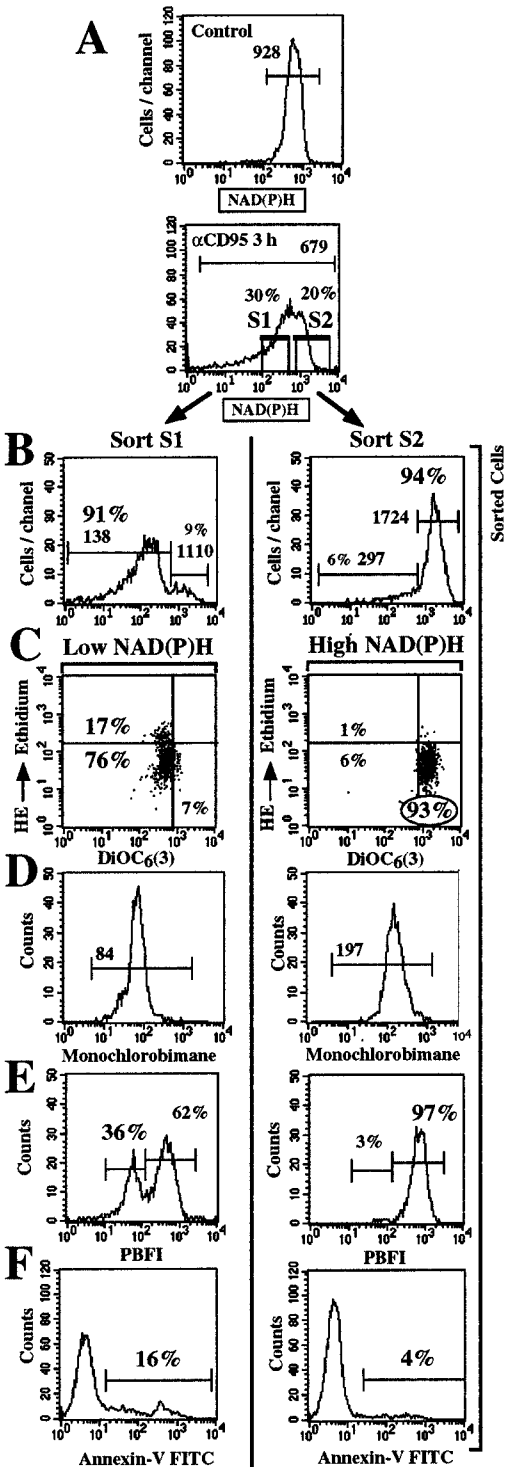

Figure 6 Apoptotic characteristics of cells as a function of their NAD(P)H content

Jurkat cells were cultured for 3 h with αCD95 and sorted using autofluorescence at 424 $\pm$ 40 nM. (**A**). The FACS-sorted cells were re-analysed for NAD(P)H-dependent autofluorescence to confirm the purification (**B**). Cells were also labelled with HE and $DiOC_6(3)$ (**C**), MCB (**D**), PBFI (**E**), and annexin V–FITC conjugate (**F**). Cells in (**C–F**) were gated on the NAD(P)H^{low} and NAD(P)H^{high} phenotype, as in (**B**).

determined using the fluorescent pH indicator SNARF-1/AM. The intracellular pH of most cells decreased as early as 3 h after stimulation with αCD95 (Figures 7A and 7B). Kinetic data

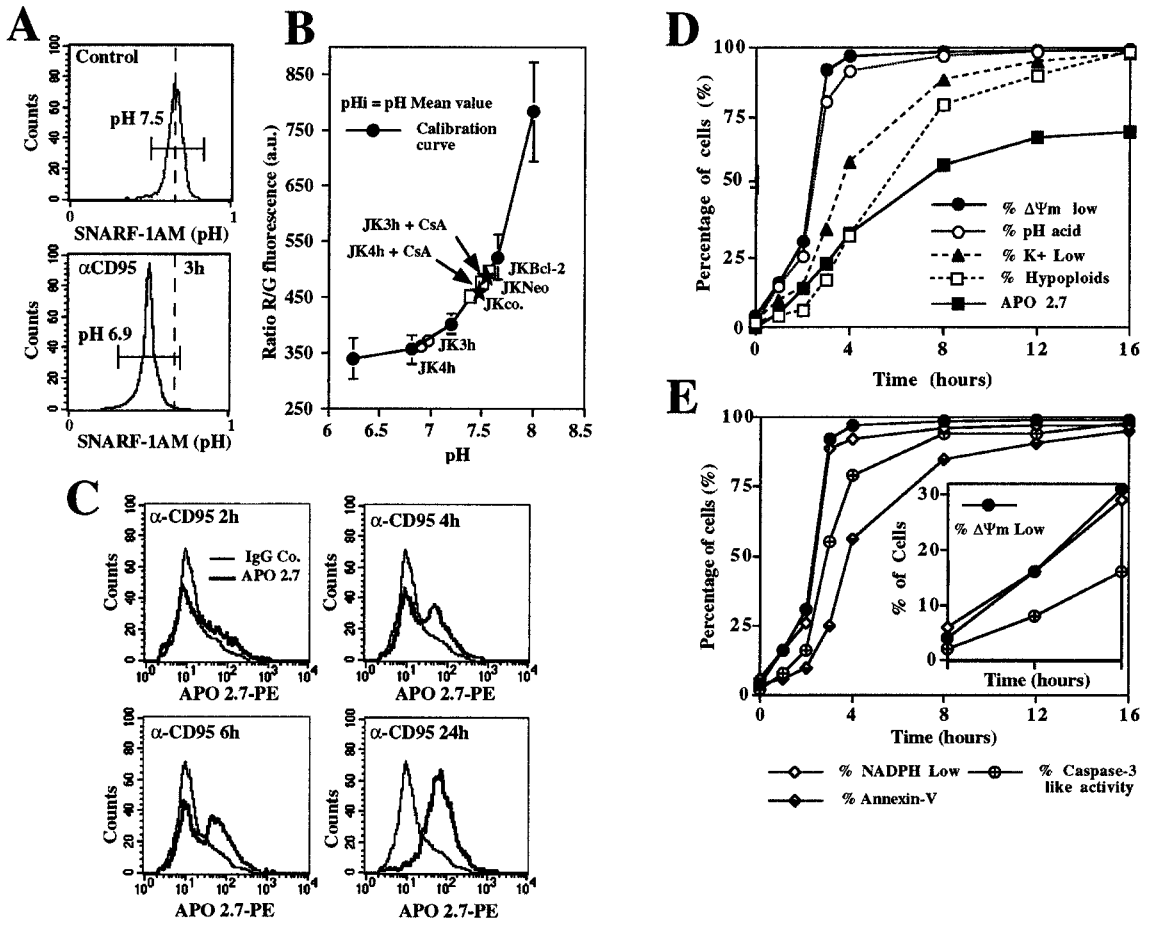

Figure 7 Intracellular pH changes during apoptosis and their kinetics

(**A**) Representative staining profiles with SNARF. Control cells or cells cultured for 3 h with 1 μg/ml αCD95 were loaded with SNARF-1/AM and the pH-dependent fluorescence ratio was measured. (**B**) Calibration curve of intracellular pH measurements. Calibration was performed with nigericin-permeabilized cells kept in buffers at different pH values [45]. The stars on the curve represent the Jurkat cells treated for 3 and 4 h with 2 μM CsA before apoptosis induction. (**C**) Representative APO2.7 staining profiles. Cells were stained at different intervals after apoptosis induction with APO2.7 or with an isotype-matched control conjugate. (**D**) Time course of pH changes and other apoptotic changes. The percentage of cells with a low intracellular pH (< 7.0) was measured as in (**A** and **B**). $\Delta\Psi_m$ collapse was measured with $DiOC_6(3)$. K^+ loss was determined with PBFI. Hypoploidy was assessed by staining ethanol-permeabilized cells with the DNA-intercalating dye propidium iodide. APO2.7 staining was performed as in (**C**). (**E**) Time course of $\Delta\Psi_m$ changes compared with the drop in NADPH and caspase-3-like cleavage activity. The inset shows the first 2 h.

(Figure 7D) confirmed the earlier observation that $\Delta\Psi_m$ collapse, GSH loss, and a drop in intracellular pH are closely related in early apoptosis [34,51]. This has also been investigated recently using a pH-sensitive green fluorescent protein [52], demonstrating that mitochondrial-matrix alkalinization and Bcl-2-inhibitable cytoplasmic acidification followed mitochondrial depolarization. These results fit well with our data provided the pH drop measured is inhibited by Bcl-2 overexpression and by CsA and BA, two of the major inhibitors of the mitochondrial PT pore (Figure 7B). NAD(P)H appears to be lost before relatively late, post-mitochondrial changes become manifest in apoptotic cells. This was indicated by experiments in which purified $NAD(P)H^{low}$ cells (obtained 3 h after adding αCD95) were re-stained with PBFI to measure the intracellular K^+ content (Figure 6E), or with annexin V–FITC (Figure 6F). Kinetic data confirmed this interpretation (Figures 6C and 6D, and Figure 7). NAD(P)H depletion occurred before the cells became subdiploid due to DNA fragmentation (measured with propidium iodide after ethanol permeabilization; Figure 7D), decreased in forward-scatter (Figure 7C), stained positively with APO2.7 (Figures 7C and 7D) or were positive for caspase-3-like activity (Figure 7E).

Functional relationship between NAD(P)H oxidation and mitochondrial PT pore opening

We determined the functional relationship between NAD(P)H loss and the early mitochondrial changes accompanying apoptosis in two series of experiments. We tested the effect of Bcl-2 overproduction (an endogenous inhibitor of PT pore opening) on NAD(P)H loss (and/or oxidization) (Figure 8B) and the effect of two pharmacological inhibitors of the PT pore, CsA and BA, on apoptosis (Figures 8A, 8B and 8C). Bcl-2, CsA, and BA retarded the loss of NAD(P)H and $\Delta\Psi_m$ dissipation. Thus $\Delta\Psi_m$ dissipation and NAD(P)H loss (and/or oxidization) were correlated even in the presence of these agents, as demonstrated by time-course analysis (Figures 8A and 8B) and by simultaneous multiparameter assessment of $DiOC_6(3)$ and NAD(P)H fluorescence in single cells (Figure 8C). This suggests that both

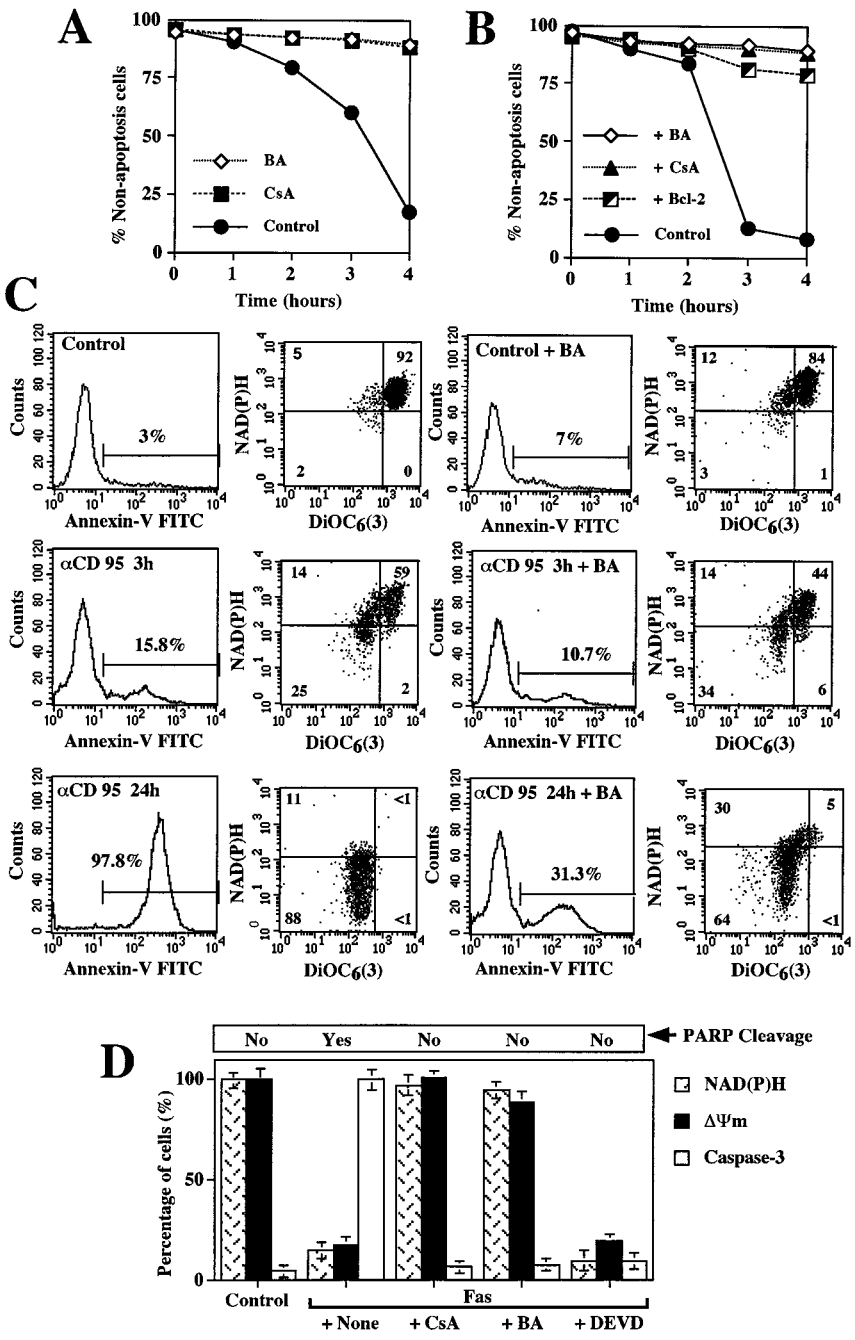

Figure 8 Effect of the PT pore inhibitors BA and CsA on $\Delta\Psi_m$ collapse and NAD(P)H loss

(**A**) Cells were treated with 0.1 μg/ml αCD95 for the indicated period in the absence (Control) or presence of 50 μM BA or 1 μM CsA, followed by determination of the frequency of cells having an apoptotic forward-scatter/side-scatter phenotype. (**B**) Kinetic data as in (**A**) for ceramide-induced apoptosis induced in the absence (Control) or presence of BA or CsA. (**C**) Representative $DiOC_6(3)$ versus NAD(P)H fluorescence profiles, and annexin V–FITC staining, of cells treated with αCD95 alone or in the presence of BA. This experiment was repeated three times, yielding similar results. (**D**) Cells were treated as in (**A**) for 4 h in the absence or presence of PT pore inhibitors CsA (1 μM) and BA (50 μM) and/or of the caspase 3 inhibitor Ac-DEVD-CHO (100 μM).

the NAD(P)H depletion and the $\Delta\Psi_m$ collapse are due to opening of the mitochondrial PT pore. Moreover, PT pore inhibitors such as CsA and BA, inhibit both NAD(P)H and $\Delta\Psi$m drop, and inhibit caspase 3 activation induced by Fas. The specific caspase 3 inhibitor Ac-DEVD-CHO inhibited caspase 3 activation, but not the NADPH and $\Delta\Psi$m drop, because caspase 3 plays a role downstream of the mitochondrial events (Figure 8D).

Temporal relationship between NAD(P)H oxidation and caspase activation

The relationship between the loss of NAD(P)H and caspase activation was determined by treating cells for 2 h with αCD95, measuring NAD(P)H and sorting them into $NAD(P)H^{high}$ cells (S1), $NAD(P)H^{intermediate}$ cells (S2) and $NAD(P)H^{low}$ cells (S3) (Figure 9A). Aliquots of the sorted populations were then stained

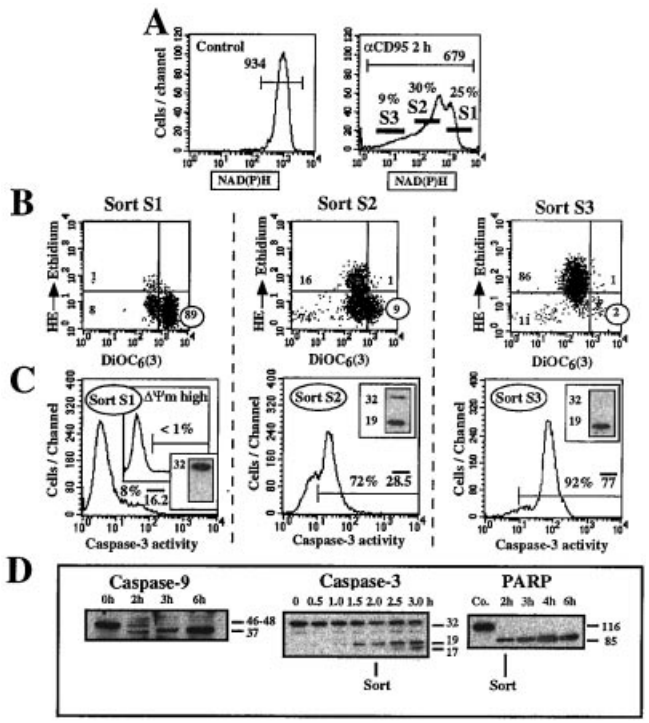

Figure 9 Relationship between NAD(P)H loss and caspase activation

(**A**) Cells were treated as indicated and analysed for NAD(P)H autofluorescence. Cells treated for 2 h with 1 μg/ml αCD95, and were sorted into NAD(P)H^{high} (S1), NAD(P)H^{intermediate} (S2), and NAD(P)H^{low} (S3) subpopulations. Aliquots of cells in S1, S2 and S3 were stained for DiOC6(3) and HE, and were analysed in (**B**). Other aliquots were incubated with the Phiphilux reagent (for 45 min at 37 °C) and were analysed in order to determine the activity of caspase 3 (**C**). The left-hand panel shows untreated control cells and the insert shows $\Delta\Psi_m^{high}$ cells from population S1. The middle panel shows data for αCD95-treated cells (0.1 μg/ml for 2 h) from population S2, and the right-hand panel shows results for the S3 cells. All three panels contain inserts showing the procaspase 3 cleavage for the S1, S2 and S3 subpopulations. (**D**) Jurkat cells were analysed by Western blots for caspase 9, caspase 3 and PARP cleavage as a function of time (caspase 3 cleavage was measured every 30 min from 0–3 h. Caspase 9 and PARP cleavage are indicated at 2 h when the cells had been sorted.

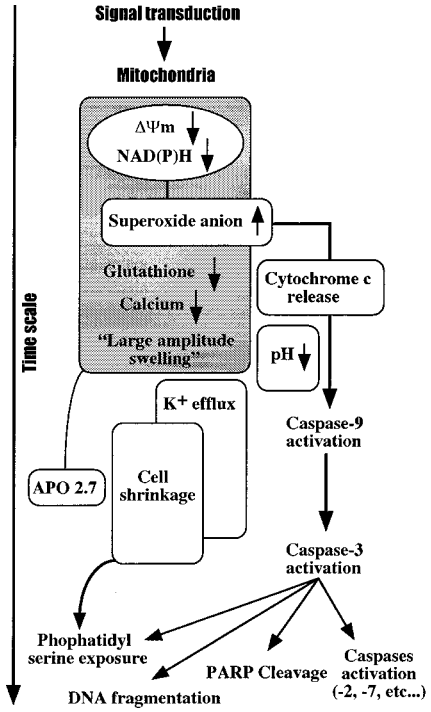

Scheme 1 Sequence of events accompanying the effector and degradation phases

NAD(P)H oxidation is strictly linked to the dissipation of $\Delta\Psi$m, and parallels GSH oxidation and cytoplasm acidification (pH decrease), but precedes superoxide generation, K^+ efflux, APO 2.7 exposure, cell shrinkage, phosphatidyl serine exposure, PARP cleavage and DNA fragmentation. Full caspase 3 activation appears to occur in the cells in which $\Delta\Psi$m decreases and superoxide anions are produced. The release of cytochrome *c* is also linked to the so-called large amplitude swelling of mitochondria.

with $DiOC_6(3)$ and HE to confirm their purity (Figure 9B). These flow-sorted populations were also stained with the caspase 3 fluorogenic substrate Phiphilux (Figure 9C). The S1 population was negative, while the S2 and S3 populations stained positively.

These results suggested that caspase 3 was activated. This was confirmed by Western-blot analysis (Figure 9D), which indicated that the S1 fraction contained only the procaspase 3 molecules (32 kDa), whereas the S2 and S3 fractions contained the 19 kDa form of proteolytically-activated caspase 3 (and also the 17 kDa form for S3). Analysis of the S2 and S3 fractions showed that the procaspase form was cleaved more in $DiOC_6(3)^{low}/HE^{high}$ cells than in $DiOC_6(3)^{low}/HE^{low}$ cells (Figure 9D). Thus the loss of NAD(P)H and the activation of caspase 3 occur almost simultaneously, while superoxide-anion positive cells contain a fully activated caspase. The caspase 9 cleavage has also been tested by Western-blot analysis and correlates with caspase 3 cleavage and activation, as does PARP cleavage (Figure 9D). Z-VAD-FMK acts similarly to Ac-DEVD-CHO (Figure 8D), and has no effect on $\Delta\Psi_m$ and NAD(P)H oxidation, but it clearly abolishes caspase 3 cleavage and activation (results not shown).

Thus our findings indicate a close chronological relationship between NAD(P)H oxidation, GSH oxidation, intracellular acidification, dissipation of $\Delta\Psi_m$, and caspase 3 activation. Major redox changes, loss of the mitochondrial-membrane barrier function, overproduction of superoxide anions and caspase 3 activation following caspase 9 activation therefore form a block of closely related changes in CD95- or ceramide-induced apoptosis of Jurkat cells. In contrast, NAD(P)H oxidation appears to precede a major efflux of K^+, cell shrinkage and phosphatidylserine exposure (Scheme 1). These data for human T lymphoma cells extend and confirm previous findings for mouse thymocytes, in which at least two clusters of apoptosis-associated alterations have been described, one early cluster involving mitochondrial changes and a decrease in GSH, and a second affecting plasma-membrane structure and function and the overproduction of superoxide anions [33,53,54].

The functional data obtained using pharmacological inhibitors of the PT pore (BA and CsA), and the genetic data obtained by transfection-enforced overproduction of Bcl-2 (which functions as an endogenous PT inhibitor), suggest that stabilization of the mitochondrial-membrane barrier function is enough to prevent the oxidation of NAD(P)H and its subsequent release from mitochondria. Similar data have been obtained in mouse thymocytes and thymoma cells, showing that BA, CsA, or Bcl-2 prevent GSH oxidation [33], and that apoptosis is a consequence of PT pore opening and the consequent mitochondrial destabilization. Conditions in which GSH and/or NAD(P)H are depleted favour mitochondrial-membrane permeabilization via

an effect that involves the PT pore [18,23,25,27,55]. Ac-DEVD-CHO inhibits caspase 3 activation, but has no effect on the $\Delta\Psi_m$ drop and NAD(P)H oxidation. Our working hypothesis is that there is a relationship between the loss of reducing equivalents and the changes in mitochondria, in which either a major shift in redox balance or a primary mitochondrial event can initiate a positive-feedback cycle of mutual amplification between PT pore opening and GSH/NAD(P)H oxidation. We do not yet know the extent to which such a positive feedback device may co-ordinate the apoptotic responses of different mitochondria within the same cell.

Hence NAD(P)H oxidation is strictly linked to the dissipation of $\Delta\Psi$m, and is concurrent with GSH oxidation and cytoplasmic acidification (pH decrease). But it precedes superoxide generation, K^+ efflux, APO2.7 exposure, cell shrinkage, phosphatidylserine exposure, PARP cleavage and DNA fragmentation. The full activation of caspase 3 appears to be restricted to the cells that show a decrease in $\Delta\Psi$m and produce superoxide anions.

Our data thus show that NAD(P)H depletion is a major component of the apoptotic pathway. A massive depletion of NAD(P)H has the same predictive value for cell death as has the dissipation of $\Delta\Psi_m$.

This work was supported by grants from the Association nationale de Recherche sur le SIDA (ANRS; to G.K.), the Association de Recherche sur le Cancer (ARC; to G.K., P.X.P. and F.S.), the Centre National de la Recherche Scientifique (CNRS), the Fondation de la Recherche Médicale (FRM; to G.K.), the Institut National de la Santé et de la Recherche Médicale (INSERM; to P.X.P., F.S. and G.K.) and the French Ministry for Science (to G.K. and P.X.P.). We also thank Beckman Coulter, Inc. for the gift of APO2.7 to P.X.P. The anti-(caspase 9) antibody was kindly provided by Dr X. Wang (Howard Hughes Medical Institute and Department of Biochemistry, University of Texas Southwestern Medical Center, Dallas, TX 75235, U.S.A.).

REFERENCES

1 Kroemer, G., Petit, P. X., Zamzami, N., Vayssière, J.-L. and Mignotte, B. (1995) The biochemistry of apoptosis. FASEB J. **9**, 1277–1287

2 Petit, P. X., Susin, S. A., Zamzami, N., Mignotte, B. and Kroemer, G. (1996) Mitochondria and programmed cell death: back to the future. FEBS Lett. **396**, 7–14

3 Petit, P. X. and Kroemer, G. (1998) Mitochondrial regulation of apoptosis. In Mitochondrial DNA mutations in aging, disease and cancer (Singh, K. K., ed.), pp. 147–165, Springer-Verlag, Berlin

4 Mignotte, B. and Vayssière, J.-L. (1998) Mitochondria and apoptosis. Eur. J. Biochem. **252**, 1–15

5 Susin, S. A., Zamzami, N. and Kroemer, G. (1998) Mitochondrial regulation of apoptosis. Doubts no more. Biochim. Biophys. Acta **1366**, 151–165

6 Vayssière, J.-L., Petit, P. X., Risler, Y. and Mignotte, B. (1994) Commitment to apoptosis is associated with changes in mitochondrial biogenesis and activity in cell lines conditionally immortalized with simian virus 40. Proc. Natl. Acad. Sci. U.S.A. **91**, 11752–11756

7 Petit, P. X., Lecoeur, H., Zorn, E., Dauguet, C., Mignotte, B. and Gougeon, M. L. (1995) Alterations of mitochondrial structure and function are early events of dexamethasone-induced thymocyte apoptosis. J. Cell Biol. **130**, 157–167

8 Zamzami, N., Marchetti, P., Castedo, M., Decaudin, D., Macho, A., Hirsch, T., Susin, S. A., Petit, P. X., Mignotte, B. and Kroemer, G. (1995) Sequential reduction of mitochondrial transmembrane potential and generation of reactive oxygen species in early programmed cell death. J. Exp. Med. **182**, 367–377

9 Castedo, M., Macho, A., Zamzami, N., Hirsch, T., Marchetti, P., Uriel, J. and Kroemer, G. (1995) Mitochondrial perturbations define lymphocytes undergoing apoptotic depletion *in vivo*. Eur. J. Immunol. **25**, 3277–3284

10 Liu, X., Kim, C. N., Yang, J., Jemmerson, R. and Wang, X. (1996) Induction of apoptic program in cell-free extracts: requirement for dATP and cytochrome *c*. Cell (Cambridge, Mass.) **86**, 147–157

11 Yang, J., Liu, X., Bhalla, K., Kim, C. N., Ibrado, A. M., Cai, J., Peng, T.-I., Jones, D. P. and Wang, X. (1997) Prevention of apoptosis by Bcl-2: release of cytochrome *c* from mitochondria blocked. Science (Washington, D.C.) **275**, 1129–1132

12 Kluck, R. M., Bossy-Wetzel, E., Green, D. R. and Newmeyer, D. D. (1997) The release of cytochrome *c* from mitochondria: a primary site for Bcl-2 regulation of apoptosis. Science (Washington, D.C.) **275**, 1132–1136

13 Petit, P. X., Goubern, M., Diolez, P., Susin, S. A., Zamzami, N. and Kroemer, G. (1998) Disruption of the outer mitochondrial membrane as a result of large amplitude swelling: the impact of irreversible permeability transition. FEBS Lett. **426**, 111–116

14 Susin, S. A., Lorenzo, H. K., Zamzami, N., Marzo, I., Snow, E. B., Brothers, G. M., Mangion, J., Jacotot, E., Costantini, P., Loeffler, M. et al. (1999) Molecular characterization of mitochondrial apoptosis-inducing factor. Nature (London) **397** 441–445

15 Green, D. R. (1998) Apoptotic pathways: the roads to ruin. Cell (Cambridge, Mass.) **94**, 695–698

16 Green, D. R. and Reed, J. C. (1998) Mitochondria and apoptosis. Science (Washington, D.C.). **281**, 1309–1312

17 Martinou, J. C., Desagher, S. and Antosson, B. (2000) Cytochrome *c* release from mitochondria: all or nothing. Nat. Cell Biol. **2**, E41–E43

18 Zoratti, M. and Szabò, I. (1995) The mitochondrial permeability transition. Biochim. Biophys. Acta **1241**, 139–176

19 Beutner, G., Rück, A., Riede, B. and Brdiczka, D. (1998) Complexes between porin, hexokinase, mitochondrial creatine kinase and adenylate translocator display properties of the permeability transition pore. Implication for regulation of the permeability transition by the kinases. Biochim. Biophys. Acta **1368**, 7–18

20 Marzo, I., Brenner, C., Zamzami, N., Susin, S. A., Beutner, G., Brdiczka, D., Remy, R., Xie, Z. H., Reed, D. and Kroemer, G. (1998) The permeability transition pore complex: a target for apoptosis regulation by caspases and Bcl-2. J. Exp. Med. **187**, 1261–1271

21 Marzo, I., Brenner, C., Zamzami, N., Jurgensmeier, J. M., Susin, S. A., Viera, H. L., Prevost, M. C., Xie, Z., Matsuyama, S., Reed, J. C. and Kroemer, G. (1998) Bax and adenine nucleotide translocator cooperate in the mitochondrial control of apoptosis. Science (Washington, D.C.) **281**, 2027–2031

22 Narita, M., Shimizu, S., Ito, T., Chittenden, T., Lutz, R. J., Matsuda, H. and Tsujimoto, Y. (1998) Bax interacts with the permeability transition pore to induce permeability transition and cytochrome *c* release in isolated mitochondria. Proc. Natl. Acad. Sci. U.S.A. **95**, 14681–14686

23 Petronilli, V., Costantini, P., Scorrano, L., Colonna, R., Passamonti, S. and Bernardi, P. (1994) The voltage sensor of the mitochondrial permeability transition pore is tuned by the oxidation-reduction state of vicinal thiols. Increase of the gating potential by oxidants and its reversal by reducing agents. J. Biol. Chem. **269**, 16638–16642

24 Costantini, P., Chernyak, B. V., Petronilli, V. and Bernardi, P. (1995) Selective inhibition of the mitochondrial permeability transition pore at the oxidation-reduction sensitive dithiol by monobromobimane. FEBS Lett. **362**, 239–242

25 Costantini, P., Chernyak, B. V., Petronilli, V. and Bernardi, P. (1996) Modulation of the mitochondrial permeability transition pore by pyridine nucleotides and dithiol oxidation at two separate sites. J. Biol. Chem. **271**, 6746–6751

26 Williams, M. D., Van Remmen, H., Conrad, C. C., Huang, T. T., Epstein, C. J. and Richardson, A. (1998) Increased oxidative damage is correlated to altered mitochondrial function in heterozygous manganese superoxide dismutase knock-out mice. J. Biol. Chem. **273**, 28510–28515

27 Nieminen, A. L., Byrne, A. M., Herman, B. and Lemasters, J. J. (1997) Mitochondrial permeability transition induced by t-buOOH:NAD(P)H and reactive oxygen species. Am. J. Physiol. **272**, C1286–C1294

28 Shinho, A., Matsuda, M., Handa, J. and Chance, B. (1998) Poor recovery of mitochondrial redox state in CA1 after transient forebrain ischemia in gerbils. Stroke **29**, 2421–2424

29 Connern, C. P. and Halestrap, A. P. (1994) Recruitment of mitochondrial cyclophilin to the mitochondrial inner membrane under conditions of oxidative stress that enhance the opening of a calcium-sensitive non-specific channel. Biochem. J. **302**, 321–324

30 Brambilla, I., Sestili, P., Guidarelli, A., Palomba, I. and Cantoni, O. (1998) Electron transport-mediated wasteful consumption of NADH promotes the lethal response of U937 cells to ter-butylhydroperoxide. J. Pharmacol. Exp. Ther. **284**, 1112–1121

31 Katoaka, A., Kubota, M., Watanabe, K., Sawada, S., Koishi, S., Lin, Y. W., Usami, I., Akiyama, Y., Kitoh, T. and Furusho, K. (1998) NADH dehydrogenase deficiency in an apoptosis-resistant mutant isolated from a human HL-60 leukemia cell line. Cancer Res. **57**, 5243–5245

32 Cai, J. and Jones, D. P. (1998) Superoxide in apoptosis. Mitochondrial generation triggered by cytochrome *c* loss. J. Biol. Chem. **273**, 11401–11404

33 Macho, A., Hirsch, T., Marzo, I., Dallaporta, B., Susin, S. A., Zamzami, N. and Kroemer, G. (1997) Glutathione depletion is an early event and calcium elevation a late event of thymocyte apoptosis. J. Immunol. **158**, 4616–4619

34 Salvemi, F., Franze, A., Iervolino, A., Filosa, S., Salzano, S. and Ursini, M. V. (1999) Enhanced glutathione levels and oxidoresistance mediated by increased glucose-6-phosphate dehydrogenase expression. J. Biol. Chem. **274**, 2750–2757

35 Dellinger, M., Geze, M., Santus, R., Kohen, E., Hirschberg, J. G. and Monti, M. (1998) Imaging of cells by autofluorescence. A new tool in the probing of biopharmaceutical effects at the intracellular level. Biotechnol. Appl. Biochem. **28**, 25–32

36 Hoffschir, F., Daya-Grosjean, L., Petit, P. X., Nocentini, S., Dutrillaux, B., Sarasin, A. and Vuillaume, M. (1998) Low catalase activity in Xeroderma pigmentosum fibroblasts and SV40-transformed human cell lines is directly related to decreased intracellular level of the cofactor, NADPH. Free Radical Biol. Med. **24**, 809–816
37 Noack, H., Kunz, W. S. and Augustin, W. (1992) Evaluation of a procedure for the simultaneous determination of oxidized and reduced pyridine nucleotides and adenylates in organic phenol extracts from mitochondria. Anal. Biochem. **202**, 162–165
38 Gellerich, F. N., Schlame, M., Bohnensack, R. and Kunz, W. (1987) Dynamic compartmentation of adenine nucleotides in the mitochondrial intermembrane space of rat-heart mitochondria. Biochim. Biophys. Acta **890**, 117–126
39 Rottenberg, H. and Wu, S. (1998) Quantitative assay by flow cytometry of the mitochondrial membrane potential in intact cells. Biochim. Biophys. Acta **1404**, 393–404
40 Kühnel, J. M., Perrot, J. Y., Faussat, A. M., Marie, J. P. and Schwaller, M. A. (1997) Functional assay of multidrug resistant cells using JC-1, a carbocyanine fluorescent probe. Leukemia **11**, 1147–1155
41 Koester, S. K., Roth, P., Mikulka, W. R., Schlossman, S. F., Zhang, C. and Bolton, W. E. (1997) Monitoring early cellular response in apoptosis is aided by the mitochondrial membrane protein-specific monoclonal antibody APO 2.7. Cytometry **29**, 306–312
42 Kasner, S. E. and Ganz, M. B. (1992) Regulation of intracellular potassium in mesangial cells: a fluorescence analysis with the dye, PBFI. Am. J. Physiol. **262**, F462–F465
43 Meuvis, K. N., Boens, F. D., De Schryver, F. D., Gallay, J. and Vaincent, M. (1995) Photophysics of the fluorescent K+ indicator PBFI. Biophys. J. **68**, 2469–2473
44 Seksek, O., Toulmé, N. H., Sureau, F. and Bolard, J. (1991) SNARF-1 as an intracellular pH indicator in laser microspectrometry, a critical assessment. Anal. Biochem. **193**, 49–54
45 Thomas, J. A., Buschbaum, R. N., Zimniak, A. and Racker, E. (1979) Intracellular pH measurement in Ehrlich ascite tumor cells utilizing spectroscopic probes generated *in situ*. Biochemistry **18**, 2210–2218

Received 26 April 2000/28 September 2000; accepted 25 October 2000

46 Nicoletti, I., Miglioratti, G., Pagliacci, F., Grignani, F. and Riccardi, C. (1991) A rapid and simple method for measuring thymocytes apoptosis by propidium iodide staining and flow cytometry. J. Immunol. Methods **139**, 271–279
47 Krippner, A., Matsuno-Yagi, A., Gottlieb, R. A. and Babior, B. M. (1996) Loss of function of cytochrome *c* in Jurkat cells undergoing Fas-mediated apoptosis. J. Biol. Chem. **271**, 21629–21636
48 Metivier, D., Dallaporta, B., Zamzami, N., Larochette, N., Susin, S., Marzo, I. and Kroemer, G. (1998) Cytofluorometric detection of mitochondria alterations in early CD95/Fas/APO-1-triggered apoptosis of jurkat T lymphoma cells. Comparison of seven mitochondrion-specific fluorochromes. Immunol. Lett. **1**, 157–163
49 Van der Heiden, M. G., Chandel, N. S., Williamson, E. K., Schumacher, P. J. and Thompson, C. B. (1997) Bcl-XL regulates the membrane potential and volume homeostasis of mitochondria. Cell (Cambridge, Mass.) **91**, 627–637
50 Rothe, G. and Valet, G. (1990) Flow cytometric analysis of respiratory burst activity in phagocytes with hydroethidine and 2′,7′-dichlorofluorescin. J. Leukocyte Biol. **47**, 440–448
51 Inai, Y., Yakubi, M., Kanno, T., Akiyama, J., Yasuda, T. and Utsumi, K. (1997) Valinomycin induces apoptosis of ascites hepatoma cells (AH-130) in relation to mitochondrial membrane potential. Cell Struct. Funct. **22**, 555–563
52 Matsuyama, S., Llopis, J., Deveraux, Q. L., Tsien, R. Y. and Reed, J. C. (2000) Changes in intramitochondrial and cytosolic pH: early events that modulate caspase activation during apoptosis. Nat. Cell Biol. **2**, 318–325
53 Castedo, M., Hirsch, T., Susin, S. A., Zamzami, N., Marchetti, P., Macho, A. and Kroemer, G. (1996) Sequential acquisition of mitochondrial and plasma membrane alterations during early lymphocyte apoptosis. J. Immunol. **157**, 512–521
54 Dallaporta, B., Hirsch, T., Susin, S. A., Zamzami, N., Larochette, N., Brenner, C., Marzo, I. and Kroemer, G. (1998) Potassium leakage during the apoptotic degradation phase. J. Immunol. **160**, 5605–5615
55 Mehendale, H. M., Roth, R. A., Gandolfi, A. J., Klaunig, J. E., Lemasters, J. J. and Curtis, L. R. (1994) Novel mechanisms in chemically induced hepatotoxicity. FASEB J. **8**, 1285–1295.